Fusing *in vivo* and *ex vivo* NMR sources of information for brain tumor classification

A R Croitor Sava[1], M C Martinez-Bisbal[2, 3], T Laudadio[1, 4], J Piquer[5], B Celda[2, 3], A Heerschap[6], D M Sima[1] and S Van Huffel[1]

[1]Department of Electrical Engineering, Division ESAT-SCD, Katholieke Universiteit Leuven, Leuven-Heverlee, Belgium

[2]CIBER of Biongineering, Biomaterials and Nanomedicine, ISC-III, Spain

[3]Departamento de Química-Física, Facultad de Química, Universidad de València, València, Spain

[4]Istituto per le Applicazioni del Calcolo "M. Picone", National Research Council, (IAC-CNR), Bari, Italy

[5]Neurosurgery Service, Hospital de La Ribera, Carretero Alzira-Corbera, Valencia, Spain

[6]Department of Neurosurgery, University of Nijmegen, University Medical Center, Nijmegen, Netherlands

Email: anca.croitor@esat.kuleuven.be

Abstract

In this study we classify short echo-time brain magnetic resonance spectroscopic imaging (MRSI) data by applying a model-based canonical correlation analyses (CCA) algorithm and by using, as prior knowledge, multimodal sources of information coming from high resolution magic angle spinning (HR-MAS), MRSI and magnetic resonance imaging (MRI). The potential and limitations of fusing *in vivo* and *ex vivo* nuclear magnetic resonance (NMR) sources to detect brain tumors is investigated. We present various modalities to combine multimodal information, study the effect and the impact of using multimodal information for classifying MRSI brain glial tumors data and analyze which parameters influence our classification results by means of extensive simulation and *in vivo* studies. Special attention is drawn to the possibility of considering HR-MAS data as a complementary data set when dealing with a lack of MRSI data needed to build a classifier. Results show that HR-MAS information can have added value in the process of classifying MRSI data.

Keywords: CCA, multimodal data fusion, brain tumor, classification, HR-MAS, MRSI

1. Introduction

Brain tumors represent an important challenge in oncology because of their relative high mortality. The World Health Organization (WHO) classification discriminates several different brain tumor types, subtypes and different grades of malignancy [1]. Additionally, brain tumors are known for their extensive heterogeneity both at the level of tumor type and grade, as well as at a microscale level, since within viable tumor tissue necrotic regions may occur and tumor cells may grow infiltrative in apparently normal brain tissue. These characteristics pose serious difficulties in the diagnosis, prognosis and treatment of brain tumors. Consequently, many researchers are now focusing on understanding this disease.

NMR techniques are widely used in the diagnosis and prognosis of brain tumors. Conventional MRI techniques focus on anatomical abnormalities and usually include proton density, T1 and T2 weighted MRI. These images essentially assess anatomy, but they are often not able to characterize the heterogeneous growth of cancer tissue and to identify tumor type or grade. To address these issues, more functional MR methods are currently being explored such as MR of vessel perfusion, of water diffusion and of metabolite distribution. In contrast to the first two, which rely on the measurement of the signal intensity of water, the latter assesses the abnormal signal levels of certain metabolites in brain tumors. This technique is called MR spectroscopy (MRS) and, if performed in a multi-voxel approach, MRSI. The latter allows the spatial mapping of metabolites and is more and more used in the clinical MR community. *Ex vivo* high resolution NMR techniques are also often considered if one is interested in an accurate biochemical profile of brain tissue, since they are very helpful for the assignment of well-resolved spectra of cellular metabolites [2]. In this context, *ex vivo* HR-MAS is seen as a promising complementary NMR technique and a good correlation between *ex vivo* HR-MAS and *in vivo* MRS has been reported [3]. Thus, HR-MAS can improve the interpretation of the metabolic biomarkers that are visible with *in vivo* NMR. Additionally, *with ex vivo* HR-MAS the tissue integrity is not extremely damaged [4] and this is an advantage since it allows one to perform, on the same tissue sample, multimodal studies including subsequent genomic, proteomic or histopathological analyses and, therefore, to obtain a direct comparison between all these techniques.

Nowadays multiple acquisitions of the brain with different techniques is getting very common. Combinatorial approaches, where different techniques are correlated or compared for assessing the tumor type and grade have been previously proposed [5-14]. These studies, where multiple data

sources are considered, can provide further insights into the biology of the brain tumors and improve the diagnosis. Still, in all these studies the multimodal sources of information are explored individually and then overlaid to demonstrate the relationship between them. It has been shown in [15-21] that fusing MRI and MRSI information improves brain tumor classification compared to the use of information of each source alone. We further explore this idea by developing a classification system for glial brain tumors where multimodal sources of information coming from HR-MAS, MRSI and MRI are integrated in the classification problem. The main purpose of this analysis is to use the common features, as well as the complementary pieces of information from our data, and therefore to simultaneously exploit metabolic and anatomical information.

In order to fuse multimodal sources of NMR information, reliable and robust classification strategies must be considered. The classification methodology proposed in this study is based on the canonical correlation analysis (CCA) algorithm [22]. CCA is an accurate and efficient statistical technique. It has been shown to be a good framework for fusing multimodal biomedical data and it has already successfully been applied to brain data [16, 21, 23-25]. CCA allows us to perform a multivariate analysis where different sources of information are integrated in the classification algorithm. Previous approaches to solve multivariate dataset problems using CCA can be classified as being either data driven such as in [23-25] or model based [16, 18, 20-21]. For this study we considered a model-based CCA approach by investigating the goodness-of-fit of the data to some prior knowledge.

Since in supervised classification one may have to deal with complications such as the limited number of samples available for analysis, we first tackle the problem of lack of data available *a priori* for building a model for our analyses based on the CCA algorithm. Then, we explore the possibility of using HR-MAS data as a complementary data set for building the models. Two different approaches of improving the classification results by fusing multimodal information are proposed: integrating multiple data sets or multi-channel modeling. Additionally, for both approaches the model accounts for inter-patient variability. To assess the quality of our method and to investigate which parameters influence the classification results, an extensive simulation study is carried out and several *in vivo* MRSI examples of brain tumor are analyzed.

2. Materials

2.1 Tumor data description

Brain tumor biopsies coming from 52 patients were provided by the acquisition centers Hospital La Ribera-Alzira (Valencia), Hospital Clínico Universitario (Valencia) and Instituto FLENI (Buenos Aires), all participating as partners in the eTUMOUR project (Web Accessible MR Decision Support System For Brain Tumour Diagnosis And Prognosis, Incorporating In Vivo and Ex Vivo Genomic and Metabolomic Data. URL: http://www.etumour.net/). Based on a histopathological study, the biopsies were assigned to three brain tumor classes: 27 cases of glioblastomas (GBM), 7 cases of grade III glioma (GIII), 18 cases of grade II glioma (GII). The tissue specimens were snap-frozen in liquid nitrogen and stored at -80^0C until the time of spectroscopic analysis, when 1D PRESAT HR-MAS (pulse-and-acquire) data were acquired. 29 out of the 52 HR-MAS experiments were conducted on a Bruker Avance DRX 600 spectrometer operating at a ^{1}H frequency of 600.13 MHz. The instrument was equipped with a 4 mm triple resonance ^{1}H/^{13}C/^{15}N HR-MAS probe with magnetic field gradients aligned with the magic angle axis. The other 23 out of the 52 samples underwent HR-MAS experiments using a Bruker Avance DRX 500 spectrometer operating at a frequency of 500.13MHz. The instrument was equipped with a 4mm triple resonance ^{1}H/^{31}P/^{13}C HR-MAS probe. A single-pulse 90^o pre-saturation experiment was acquired in all the samples. To keep the rotation sidebands out of the acquisition window, samples were spun at 5000 Hz in the DRX 600 spectrometer and at 4000 Hz in the DRX 500 spectrometer. The HR-MAS signals were truncated from 8120 points to the first 2048 points to reduce the computational load in the pre-processing steps. The water components were removed by HLSVD-PRO [26]. The filtered signals were normalized (divided by the Euclidean norm of the frequency domain signal within the region of interest between 0.25 and 4.2 ppm) and aligned with respect to the Alanine doublet at 1.47 ppm. A baseline correction was applied using an apodization function in the following way. The signal was point-wise multiplied in the time-domain with an exponentially decaying function. Then, the resulting spectrum mainly contained the broad baseline components, which were subsequently subtracted from the original spectrum, yielding the preprocessed signal.

Histopathological analysis on the same tissue part used in the HR-MAS experiment revealed a high variability in the content of highly cellular tumor tissue, infiltrations with normal tissue and/or necrotic tissue. Since a strong correlation between the histopathological tissue properties and the metabolic profiles coming from *ex vivo* HR-MAS was observed [27], in order to avoid large variations within the samples belonging to the same brain tumor class we excluded those tumor

samples with high infiltration from normal tissue. Thus, for the statistical analyses we considered 13 GII, 5 GIII and 22 GBM HR-MAS measurements.

MRSI data of 24 patients with brain tumor were considered. Both water suppressed and unsuppressed proton MRSI data were acquired in the Radboud University of Nijmegen Medical Centre (RUNMC) on a 1.5T clinical MR system (Siemens Vision), using a 2D STEAM pulse sequence with the STEAM box positioned in a transversal plane through the brain showing the largest tumor diameter in the Gd contrast enhanced image. The MRSI parameters are: 16x16x1024 samples, TR/TE/TM=2000 or 2500/20/30 ms, slice thickness = 12.5 or 15 mm, FOV (field of view) = 200 mm, spectral width = 1000 Hz and NS=2. The study was approved by the ethical committee of the UMCN and for tumor typing followed the rules of the World Health Organization (WHO). Thus, each patient's tumor was diagnosed based on a histopathological study and 176 spectra for GII, 57 spectra for GIII and 70 GBM spectra could be extracted from the 24 cases. The water suppressed MRSI signals were preprocessed as follows: filtering of k-space data by a Hanning filter of 50% using the LUISE software package (Siemens, Erlangen, Germany), zero filling to 32 x 32 and spatial 2D Fourier transformation to obtain time domain signals for each voxel, eddy current correction, water removal with HLSVD-PRO [26] and baseline correction performed as described in [28]. Zero-order phase was already corrected during eddy current correction. Manually, all first order phases were adjusted. Finally, all spectra were normalized with respect to the unsuppressed water signal.

For each of the 24 patients 4 MR images were acquired: T1 weighted (TE/TR=15/644ms), T2 weighted (TE/TR=16/3100ms), proton density weighted (TE/TR=98/3100ms) and Gadolinium enhanced T1 (15 ml 0.5 M Gd-DTPA).

3. Methods

3.1 Harmonization of the input spaces

The fusion of multimodal data sets is a challenging problem since the data are dissimilar in nature. To overcome this problem we propose a feature-based approach. For harmonizing the spectral MRSI and HR-MAS information, a dimension reduction of the available data is performed, by quantifying the most important metabolite concentrations using peak integration applied to the preprocessed signals. The following 10 metabolites were considered: *Lip1* (lipids at *0.9ppm*), *Lip2* (lipids at 1.3 ppm), *Lac* (lactate), *Ala* (alanine), *NAA (*N-acetyl-aspartate), *Glx group* (glutamine -

Gln and glutamate - *Glu*), *Cr* (creatine), *Cho* (choline), *Tau* (taurine), *mI* (myo-inositol) + *Gly* (glycine). The chosen metabolites are important biomarkers for separating different tissue types within the brain and present a high correlation in *ex vivo* and *in vivo* measurements [3].

The linewidth and SNR differences between *in vivo* and *ex vivo* spectra, see figure 1, makes us reasonably think that different strategies are required to extract relevant features. Thus, different integration intervals are considered for HR-MAS and MRSI spectra, respectively (see table 1).

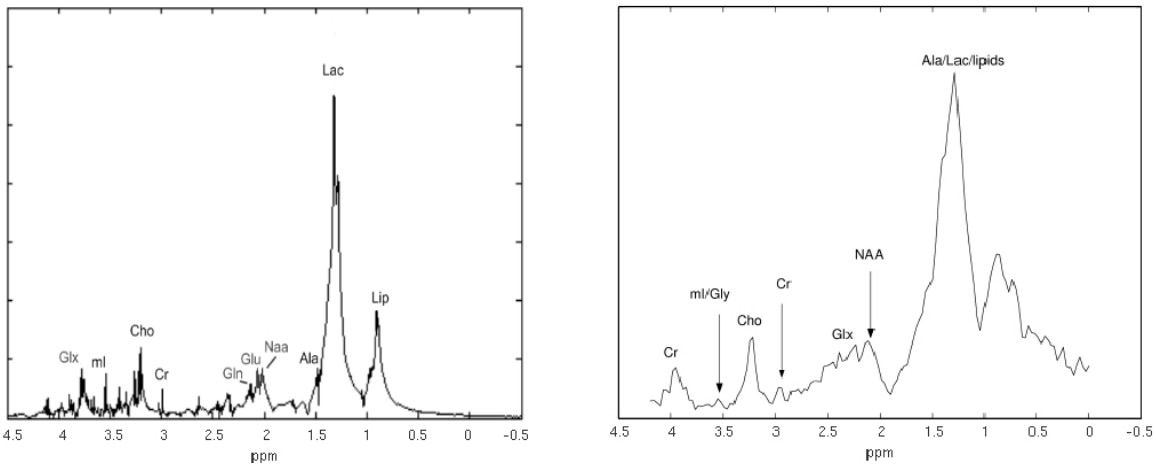

Figure 1. Comparison between an ex vivo spectrum (left) and an in vivo spectrum (right) for GBM. The vertical axes are scaled in order to facilitate a visual comparison and the displayed frequency region is the area of interest [0.25, 4.2] ppm.

Due to peak overlap and relatively low spectral resolution that characterize the MRSI measurements at the clinical field strength considered in this study, *Lac, Ala* and *Lip2* were extracted as one feature, *Glu* and *Gln* were also grouped, the same for *mI* and *Gly*, as well as *Glu, Gln* and *Ala,* which overlap around 3.74 ppm.

For HR-MAS, the considered metabolites were quantified separately. Peaks which were grouped together in short-echo time ^{1}H MRSI spectra were grouped in the same manner in HR-MAS spectra, by summing up their corresponding integrated area into one feature.

Table 1. Integration intervals: MRSI vs HR-MAS spectra.

Metabolite	MRSI	HR-MAS
Lip1	[0.835-0.965] ppm	[0.860-0.920] ppm
Lac + Ala +Lip2	[1.265-1.395] ppm	[1.320-1.340] ppm (Lac) [1.450-1.490] ppm (Ala) [1.300-1.320] ppm (Lip)
NAA	[1.955-2.085] ppm	[1.955-2.085] ppm
Glu+Gln	[2.135-2.265] ppm	[2.090-2.170] ppm (Gln) [2.390-2.50] ppm (Glu)
Cr	[2.955-3.095] ppm	[3.010-3.030] ppm
Cho	[3.135-3.265] ppm	[3.135-3.245] ppm
Tau	[3.375-3.505] ppm	[3.390-3.420] ppm
mI+Gly	[3.495-3.625] ppm	[3.500-3.620] ppm
Glu+Gln+Ala	[3.685-3.815] ppm	[3.720-3.800] ppm
Cr	[3.885-4.015] ppm	[3.910-3.940] ppm

The obtained metabolite concentrations for each spectrum are then stacked into a vector, which we call a feature vector. In this way we obtain a database containing MRSI feature vectors, S_{MRSI} , and one with HR-MAS feature vectors, S_{HR-MAS} , for each tissue type.

Spectral information is also combined with imaging information coming from MRI measurements and the harmonization of these sources is performed, as described in [17], by lowering the resolution of the MR images to the MRSI voxel size. Specifically, the images with 4 contrasts are aligned with respect to the spectroscopic image and the MR pixel intensities are averaged out over a spectroscopic voxel obtaining 4 additional variables. This information is gathered in a database of feature vectors for MRI data, S_{MRI} , for each tissue type.

Finally the resulting MRSI, HR-MAS and MRI feature vectors are scaled to be in the same numerical range. More precisely, the arithmetic mean of each feature vector is subtracted from its elements, so that the new elements are centered around zero, and the new vector is scaled by division to its Euclidean norm.

3.2 Canonical Correlation Analysis

To illustrate the idea of fusing *ex vivo* HR-MAS, *in vivo* MRSI and MRI features we considered a model-based approach of the statistical method CCA, which has recently been successfully applied to classify prostate and brain MRSI data [16, 20, 21].

CCA is a multi-channel generalization of ordinary correlation analysis, which quantifies the relation between two random variables by means of the so-called correlation coefficient:

$$\rho = \frac{Cov[x, y]}{\sqrt{V[x] * V[y]}} \tag{1}$$

where *Cov* stands for covariance and *V* for variance, and *x* and *y* denote here two scalar random variables. CCA seeks two sets of transformed variates such that the transformed variates assume maximum correlation across two data sets. Being a multivariate method, it can provide increased statistical power over univariate methods. It can be applied to multichannel signal processing as follows: consider two zero-mean multivariate random vectors $x = [x_1, \ldots, x_m]^T$ and $y = [y_1, \ldots, y_n]^T$, where the superscript *T* denotes the transpose. We define the following linear combinations of the components of *x* and *y*, which represent two new scalar random variables X and Y:

$$\begin{aligned} X &= \omega_{x_1} x_1 + \cdots + \omega_{x_m} x_m = \omega_x^T x \\ Y &= \omega_{y_1} y_1 + \cdots + \omega_{y_n} y_n = \omega_y^T y \end{aligned} \tag{2}$$

CCA computes the coefficients $\omega_x = [\omega_{x_1}, \ldots, \omega_{x_m}]^T$ and $\omega_y = [\omega_{y_1}, \ldots, \omega_{y_n}]^T$, known as regression weights, that maximize the correlation between the so called canonical variates X and Y. Nonnegativity constraints on ω_x and ω_y are imposed, as in [29].

3.2.1 Model-based CCA. During an MRSI acquisition, spectra are measured in a grid of voxels. Inspired by [16], we want to assign each voxel to a certain tissue type by computing the maximum canonical correlation coefficient between the information available for the voxel of interest (*x*) and the tissue models obtained based on the information available a priori (*y*). Since we believe that there is a high probability that the voxel under investigation belongs to the same tissue type as the

neighboring voxels, when defining the *m* components of *x* we include spatial information coming from the voxels surrounding the voxel of interest. To this aim a symmetric 3x3 spatial model was considered (the adjacent voxels plus voxels on the diagonal are considered as neighbors, giving a total of 8 voxels). This means that, for example, for classifying the voxel on position 5 shown in figure 2, where for each position *i* we denote the corresponding feature vector with x_i, we compute the *x* variable as:

$$x = [x_5, (x_1 + x_9)/2, (x_2 + x_8)/2, (x_3 + x_7)/2, (x_4 + x_6)/2]^T$$

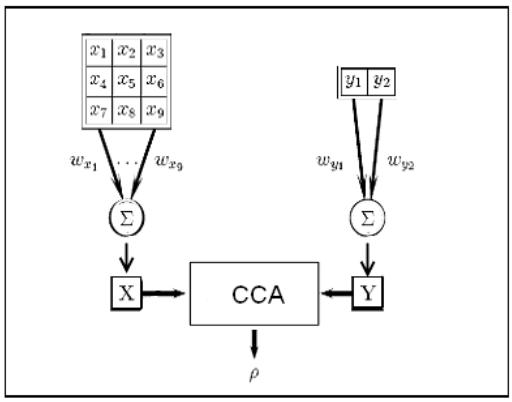

Figure 2. Schematic representation of CCA when applied to a 3x3 region of MRSI voxels

Since for each voxel we have access to two data sets of measurements, i.e. MRSI and MRI information, x_i, where $i = 1,\ldots,9$, is defined as a feature vector containing 14 entries by concatenating 10 metabolite estimates extracted from the spectrum of the $i-th$ voxel and 4 image intensities extracted as described in Section 3.1, alongside each other.

The *y* variable represents the so-called subspace model and is defined by two vectors:

$$y = \begin{cases} y_1 = [\overline{S}, \overline{S}_{MRI}] \\ y_2 = [1^{st} PC_{[\widetilde{S}, \widetilde{S}_{MRI}]}] \end{cases} \quad (3)$$

where $\overline{S}$ represents the mean of all the considered spectral feature vectors, extracted from the a priori available database of validated S_{MRSI} and/or $S_{HR\text{-}MAS}$ data, and $\overline{S}_{MRI}$ the mean of all the available S_{MRI} data. Thus, y_1 consists of 14 entries: 10 spectral feature vectors and 4 image intensities concatenated alongside each other. In order to model the natural inter-patient variability,

a second component (y_2) is defined as the first principal component, 1st PC, obtained by performing principal component analysis (PCA) separately on the matrices $\widetilde{S}$ and $\widetilde{S}_{MRI}$ obtained by mean centering the previously considered matrices *S* and $S_{MRI.}$ For each tissue type we defined a distinct subspace model by considering only the a priori available information belonging to the same tissue type.

Once x and y have been defined, CCA is applied to each voxel so that a correlation map is obtained for each tissue type. These correlation maps are then compared, assigning to each voxel the tissue type corresponding to the largest canonical correlation coefficient. In this way nosologic images are constructed such that all voxels of the same tissue type are visualized with the same color [30]. These images can be easily interpreted by radiologists and physicians and, along with clinical and radiological information, can improve the accuracy of the diagnosis.

3.3 Simulation study

Firstly, for the simulated MRSI experiment, the available MRSI dataset is randomly split into two sets: one test set used for building simulated MRSI grids and one set to build the tissue subspace models. Thus, representative information coming from multi-voxel MRS measurements for the different glial tumor types and normal tissue is used to simulate 10x10 MRSI grids. All grids present two tissue regions: a region of 5x5 tumor voxels in the upper left corner and normal tissue in the remaining ones. The artificial MRSI data (see figure 3) are created by making use of a set of vectors consisting of 14 features (10 metabolite concentrations and 4 image intensities). CCA is then evaluated on 30 grids, namely on 10 different images for each tumor type (GII, GIII and GBM).

Figure 3. Feature vectors of a simulated MRSI grid. Left upper corner square (red contour): GBM tissue; rest of the grid: normal tissue.

Each voxel within the simulated MRSI grids is classified using CCA and the performance of the classification is evaluated by computing the area accuracy rate (AAR) and the weighted accuracy rate (WAR) [31, 32], as defined in (4) and (5). The former value provides information on the degree of reliability of the method in detecting the tumor region; the latter provides information on the method's ability in differentiating the tissue types characterizing the lesion, i.e. in assigning each voxel to the right tissue class.

$$AAR = \left(\frac{a+b+c+d}{A+B+C+D} \right) \tag{4}$$

$$WAR = \frac{1}{N}\left(\frac{a}{A} + \frac{b}{B} + \frac{c}{C} + \frac{d}{D} \right) \tag{5}$$

where a, b, c and d represent the number of correctly predicted outcomes for normal, GII, GIII and GMB tissue respectively. A, B, C and D represent the number of cases belonging to normal, GII, GIII and GBM, respectively. N is the total number of classes (in our case N = 4).

3.3.1 CCA performance for different size of the database used in building the tissue subspace model. We analyze the behavior of CCA for different database dimensions used in building the tissue subspace model. When defining *y,* MRSI and MRI information is considered [16], see (3), with $S = [S_{MRSI}]$, (MR imaging features, $S_{MRI,,}$ are included as well). We tested the performance of

CCA when considering large database of cases to build the tissue subspace models by using all the available MRSI and MRI data (i.e. 176 cases for GII, 57 cases for GIII, and 70 cases for GBM) and, then, gradually reducing the size of the database to a very small number of cases (10 cases of GII, 10 cases of GIII and 10 cases of GBM tumor).

3.3.2 Adding complementary information coming from HR-MAS. In this part of the study we tackle the problem of lack of data needed to build the subspace models by analyzing to which extent HR-MAS can help in improving the classification results, when this problem is encountered. One approach is to merge MRSI and HR-MAS information in one single database by stacking the feature vectors extracted from the two types of spectra into one matrix, $S = [S_{MRSI_{1...10}}; S_{HR-MAS}]^T$, and afterwards to compute the subspace mode y as defined in (3), including the MR imaging features, $S_{MRI,}$ as well. This approach is further called *data integration*.

Another approach is to consider different channels of multimodal sources of information coming from both the MRSI and HR-MAS datasets when computing *y*. Thus, a subspace model from each data source is computed separately and then both are merged into a final subspace model. We then obtain a subspace model where the y variable now contains 4 components, 2 coming from the MRSI data and 2 coming from the HR-MAS database:

$$y = \begin{cases} y_1 = [\overline{S}_{MRSI}, \overline{S}_{MRI}] \\ y_2 = 1^{st} PC_{[\widetilde{S}_{MRSI}, \widetilde{S}_{MRI}]} \\ y_3 = [\overline{S}_{HR-MAS}, \overline{S}_{MRI}] \\ y_4 = 1^{st} PC_{[\widetilde{S}_{HR-MAS}, \widetilde{S}_{MRI}]} \end{cases} \quad (6)$$

This modality of computing the subspace model is further referred to as *multichannel approach*.

The performance of CCA for the two approaches considered in building the subspace model is analyzed and compared for various scenarios where HR-MAS information is added gradually. Thus, various combinations of (l_1,l_2), where l_1 represents the number of MRSI cases and l_2 the number of HR-MAS cases, are considered in the subspace model: (0,0), (5,0), (10,0), (all,0), (0,10), (5,10), (10,10), (all,10), (0,30), (5,30), (10,30), (all,30), (0,all)), (5, all), (10,all), (all, all).

3.4 In vivo study

In order to verify to which extent the conclusions drawn in the simulation studies are consistent with real conditions, we further test the above described approaches on real-life case studies. As already described in Section 3.2, CCA assigns each voxel to a histopathological class based on the highest canonical correlation coefficient value. We draw nosologic images, where each voxel is colored according to the tissue class it belongs to as follows: dark blue is used for normal tissue, and yellow, red and orange are used to color the tumor voxels, each color representing a different tumor type (GII, GIII and GBM, respectively).

The results obtained by all considered approaches used in building the subspace model are reported and compared against the clinical outcome.

4. Results

4.1 Simulation study

4.1.1. Influence of the size of the database used to build the tissue subspace model. A decrease in performance is observed when building the subspace models from a small number of cases, see figure 4. In particular, the WAR value presents a decrease from 91.4 % (when using a database with more than 50 cases) to 76.2% (when using a database containing 10 cases) when analyzing the GII simulated MRSI grids. Generally, the accuracy of the classifier shows to be positively correlated to the number of available cases used to build the subspace model: the more cases we include, the better performance we achieve.

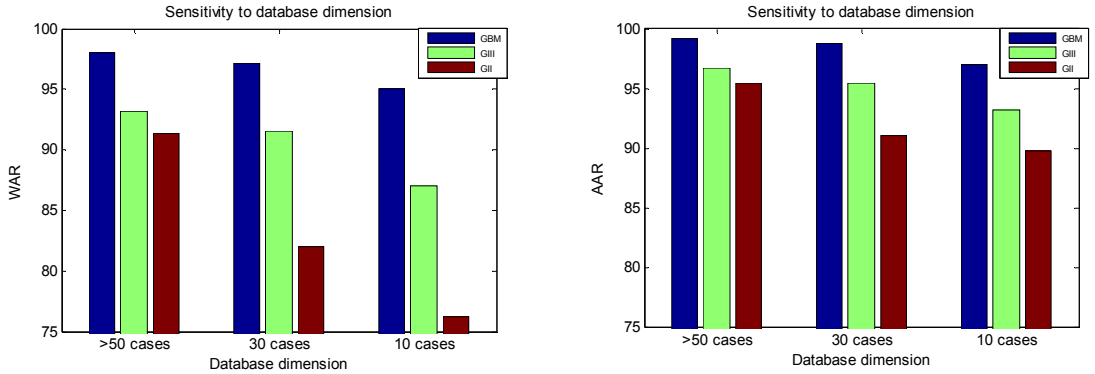

Figure 4. WAR (left) and AAR (right) mean values obtained over 10 simulated MRSI grids are presented for different database sizes used to build the tissue subspace models.

4.1.2. Adding HR-MAS information when building the subspace model. Results show that both approaches considered for adding complementary HR-MAS information when building the subspace model, *data integration* and *multichannel approach*, respectively, improve CCA classification results when not enough MRSI data are available. Especially for the GII case we get an improvement in accuracy up to 8% when adding extra information coming from HR-MAS, compared to the case when considering a database of 10 or less MRSI data, see figure 5. For the GIII case, the increase in accuracy is not significant. This can be explained by the fact that we have a set of only 5 HR-MAS signals for this type of tumor. Therefore, even by complementing the 10 cases of the MRSI data set with 5 new HR-MAS cases, we are still dealing with a small database.

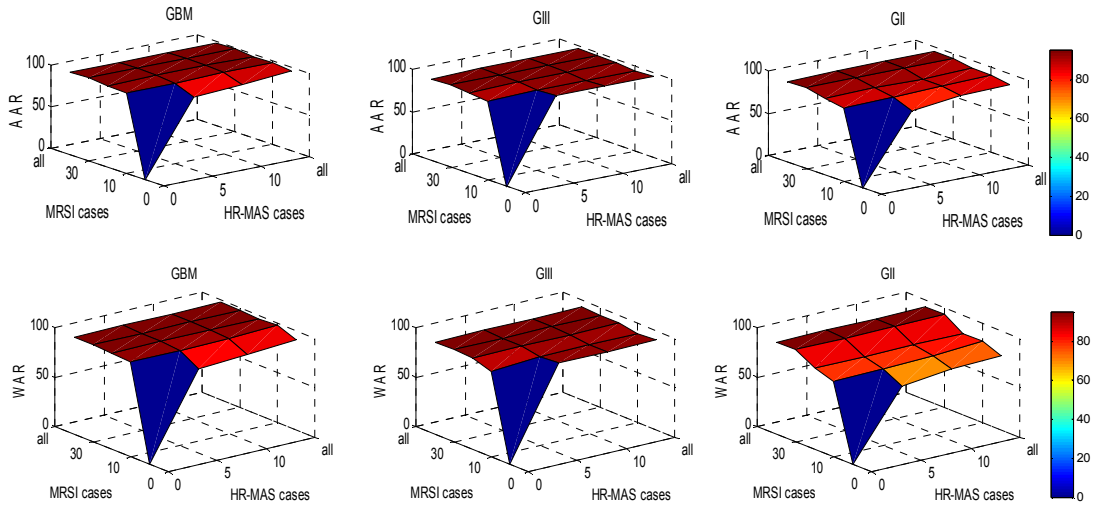

Figure 5. AAR (top) *and WAR (bottom) mean values obtained over 10 simulated MRSI grids for different number of MRSI and HR-MAS cases considered in building the subspace model. Data integration approach was considered in building the subspace model. (For GIII we have a total of 5 HR-MAS cases and, therefore, the values are not changing through the plot for HR-MAS when considering 10 and all cases.)*

The general trend is that when not enough information of one source (e.g. MRSI) is available in the database for one or more tissue classes, then, using complementary information coming from HR-MAS data when building the subspace model keeps the performance of CCA to a reliable level. On the other hand, when sufficiently large data sets of one source (e.g. MRSI) is available in the database for one or more tissue classes, then adding extra HR-MAS information to the MRSI data sets does not bring any statistical significant improvement to the classification results when considering the *data integration* approach. On the contrary, with the *multichannel approach* for GII

tumor classification we obtain an increase in the WAR value to almost 96%, see figure 6. This could be due the fact that by considering *a multichannel approach* when building the subspace model a four-dimensional subspace, as in eq. (6) is built, instead of a two-dimensional subspace (3). Consequently, 4 coefficients ω_y instead of only 2 are optimized such that the correlation between X and Y is maximized. This offers more flexibility in exploring all correlations between the data and each of the two types of information used for building the model.

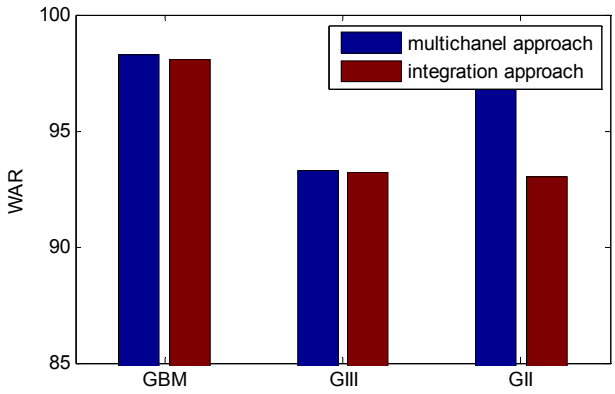

Figure 6. WAR values for different tumor types: comparison between the multichannel approach and data integration approach when considering large MRSI and HR-MAS data sets.

When using only HR-MAS data to compute the tissue subspace models (in figure 5, note the values corresponding to 0 MRSI cases), the accuracy of the classifier is relatively high, especially for classifying GIII and GBM tumor types. The performance for this specific case does not reach the level of performance obtained with a subspace model computed from large representative MRSI data sets (compare in figure 5 the values corresponding to the scenario (0, all) against (all, 0). Still, taking into consideration the fact that we use totally different data sets coming from different centres and acquired with different techniques (HR-MAS data for building the model and MRSI data for testing the performance), we believe that these results show the potential of using heterogeneous sources of information for tissue typing (e.g. in brain tumor recognition) which is particularly interesting when no information of one source (e.g. MRSI) is available for one or more tissue classes. We prove that using only HR-MAS data we can build a reliable classifier that is able to provide satisfactory results for classifying MRSI data. We show once more that these two NMR techniques (HR-MAS and MRSI) can complement each other. For the GII tumor, the performance of CCA is lower than for the other two tumor types. We believe that there are many factors that can

explain these results. First of all, when analyzing tissue samples, i.e. HR-MAS data, the sampling procedure is crucial for homogeneity. In most NMR experiments, pH and temperature must be tightly regulated to ensure homogeneity across peak positions and amplitude, as there is a strong dependence between a spin resonance frequency and its local environment [33]. Some experimental variables, like the effects of changing the sample volume in the MAS rotor, snap-freezing the samples, the temperature could have an influence on the estimated concentration of some metabolites. On the other hand, the variability among the glial tumor spectra may be large due to the fact that the same type of tumor may include molecular subgroups which may greatly affect the concentrations of some metabolites.

4.2 In vivo studies

figure 7.a shows the T2 MRI image of a brain affected by tumor. The patient is diagnosed with low grade astrocytoma, GII. The tumor lesion is localized in the left upper corner of the MRSI grid. The results obtained with CCA are translated into nosologic images and are presented in figure 7.b-e. The area of the tumor is correctly detected by all the considered approaches (CCA where only MRSI cases are used in building the model, only HR-MAS cases are used in building the model, all MRSI and HR-MAS cases are used in building the model with *data integration approach* and all MRSI and HR-MAS cases are used in building the model with *multichannel approach* for 7.b, 7.c, 7.d ,and 7.e respectively) and no isolated tumor voxels appear in the healthy tissue area. Regarding the accuracy level for detecting the tumor type, differences can be noticed between the considered approaches. Both 7.b and 7.c assign some voxels to GIII. This can be explained by the fact that the spectra within these voxels present higher levels of Cho and lower levels of NAA compared to the rest of the tumor area, which is typical for aggressive grade tumor and/or high cellularity tumor tissue. In 7.d the entire area of the tumor is assigned to GII. Still, some voxels of normal tissue are detected inside the area of the tumor. The result closest to the clinical validation is the nosologic image obtained for 7.e.

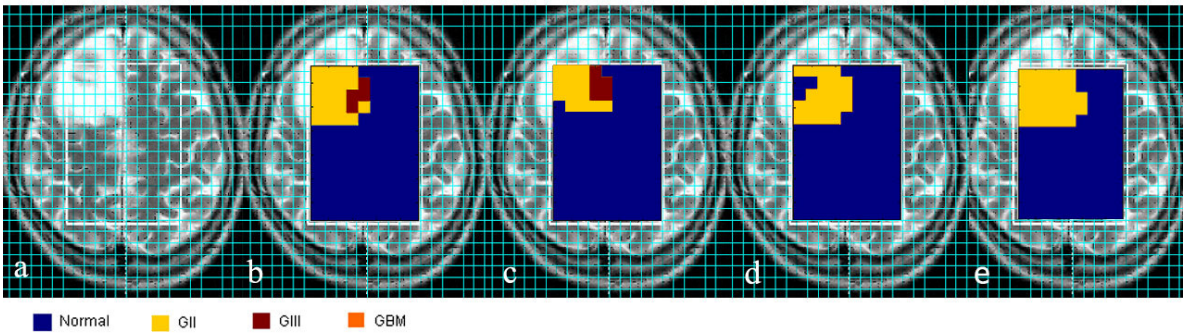

Figure 7. a. T2 MRI image of a brain affected by tumor; nosologic images obtained CCA for b. all MRSI cases used in building the subspace model, c. only HR-MAS cases are used in building the model, d. all MRSI+HR-MAS cases are used in building the model with data integration approach e. all MRSI and HR-MAS cases are used in building the model with multichannel approach

The CCA performance for the real-life case studies is similar to the performance obtained in the simulated studies and results are in consensus with the clinical outcome.

5. Discussion

For this study, as we had access to three different sources of information, the input space (i.e. prior available database) could be either spectral information coming from MRSI data, information coming from HR-MAS spectra, a set of image intensities coming from MRI data, or the combination of all described sources. It is very common to consider a classification using these sources separately. Since each of the input data source can add extra information to the classification problem, a multimodal approach fusing all the information seemed as a reasonable solution in this study. Previous studies have shown that, when classifying MRSI data, a significant improvement in the performance of the classifier is obtained by taking into account MRI information as well [16-21]. We further explored this idea by analyzing the behavior of a classification method that combines three sources of multimodal information.

A challenging problem in this study was the harmonization of all the input spaces due to the fact that we have to manage the use of very different sources of information/data, obtained with different measurement techniques, as well as the use of data coming from different clinical centers. The problem was overcome by considering a feature-based CCA approach, where common

characteristic features from all the different data types are extracted and a normalization of the data was performed.

Since the performance of the model-bases CCA algorithm proposed for this study is directly dependent on the prior available observations used in building the model, special attention is paid to the possibility of using HR-MAS data as a complementary data set when dealing with a lack of MRSI data needed to build a classifier. It is worthwhile to stress that the model choice dictates the detection performance. In general, when working with supervised classification methods, the classifier has to learn the significant features, by means of a training procedure, to separate the different classes. Thus, in order to obtain reliable classifiers we need large and representative datasets for each class. Nevertheless, some clinically important tumors are sufficiently rare that even a large multicentre study would be unlikely to gather sufficient cases to define their metabolite profiles using *in vivo* MRS. Therefore, for rare brain tumors little is known biologically and a diagnosis on the basis of morphologic and metabolic appearance alone is controversial. Nowadays, large collaborative programmes exist for collecting frozen tissue from such tumours at surgery and placing them in a tumor bank. Biological studies using frozen tissues from tumor banks have been highly successful and HR-MAS could form part of such a study. We evaluate the CCA performance when solving the aforementioned problem either by adding HR-MAS data to the *in vivo* database, or considering only HR-MAS data sets for building the subspace model, see Section 3.2. This approach promises to be an interesting solution when only a limited number of MRSI cases are available to build the subspace-models. Results of this study show that determining metabolite concentrations from the tissue samples with HR-MAS and using this information to define the MRS metabolite profiles found *in vivo* can help to the construction of *in vivo* MRS classifiers. We have explored two approaches for building the model that combines both sources of information. *Data integration approach* is a straightforward approach where no distinction is made between the sources of information, because the extracted features are treated in common. That is, feature vectors from MRSI and from HR-MAS are grouped into a single dataset, from which the mean and the first principal component are extracted as model y. This approach might lose specificity in the case when there is some incongruence between the two sources of information. Therefore we introduced a second approach, the *multichannel approach*, where the two sources of data are not averaged together, but are considered as different directions to which the data to be classified might align to. We have seen that this approach led to a better classification of the simulated GII cases.

The idea presented in this study can be extended to any type of tumor, especially to the rare ones for which a biopsy is normally performed, and to any pattern recognition method/system that makes use of a learning procedure or uses reference tissue models. This could be very interesting for distinguishing between rare tumours and between rare and common tumours of clinical importance. Such a system can afterwards be applied to classify other MRSI data non-invasively, thereby avoiding the need of new biopsies.

6. Conclusions

Fusing multimodal sources of information coming from MRSI, HR-MAS and MRI measurements represents a promising approach to provide improved detection and classification of brain tumors since each source has its own advantages and limitations and, therefore, they can complement each other. This approach can add value to the process of tumor diagnosis, both for the situation when we are confronted with a lack of information available for building a classifier as well as for the situation when we have access to different sources of information and we use all these sources in building a robust classifier. Additionally, results show that HR-MAS information can act as an added value in the process of classifying MRSI data. An improvement in the accuracy of CCA is observed for all tissue types when a limited number of MRSI data, needed to build the subspace model, are available in the database and HR-MAS data are used as a complementary data set. Moreover, our simulation and *in vivo* studies show that when we have access to various type of information describing the same population, combining multimodal heterogeneous sources of information can also improve the performance of CCA in detecting correctly the tumor type and the tumor region.

Acknowledgements

This research is funded by the EU projects eTUMOUR (FP6-2002-LIFESCIHEALTH 503094) and Healthagents (IST–2004–27214). The authors acknowledge EU for the use of data provided by INTERPRET project (contract no. IST-1999-10310).

Research supported by

- Research Council KUL: GOA Ambiorics, GOA MaNet, CoE EF/05/006 Optimization in Engineering (OPTEC), PFV/10/002 (OPTEC), IDO 05/010 EEG-fMRI, IDO 08/013 Autism, IOF-KP06/11 FunCopt, several PhD/postdoc & fellow grants;
- Flemish Government:

- FWO: PhD/postdoc grants, projects: FWO G.0302.07 (SVM), G.0341.07 (Data fusion), G.0427.10N (Integrated EEG-fMRI) research communities (ICCoS, ANMMM);
- IWT: TBM070713-Accelero, TBM070706-IOTA3, TBM080658-MRI (EEG-fMRI), PhD Grants;

- Belgian Federal Science Policy Office: IUAP P6/04 (DYSCO, `Dynamical systems, control and optimization', 2007-2011);ESA PRODEX No 90348 (sleep homeostasis)
- EU: FAST (FP6-MC-RTN-035801), Neuromath (COST-BM0601)

Ministerio Ciencia e Innovación de España projects: SAF2007-65473; SAF2007-29393-E; SAF2007-29394-E; SAF2007-29455-E

National Research Council of Italy, Short Term mobility Program, 2008

References

1. Louis DN, Ohgaki H, Wiestler OD, Cavenee WK. World Health Organization Classification of Tumours of the Central Nervous System. IARC, Lyon, 2007, ISBN 9283224302.

2. Martıinez-Bisbal MC, Martıi-Bonmati L, Piquer J, Revert A, Ferrer P, Llacer JL, Piotto M, Assemat O and Celda B. ^{1}H and ^{13}C HR-MAS spectroscopy of intact biopsy samples ex vivo and in vivo ^{1}H MRS study of human high grade gliomas. NMR Biomed. 2004;17(4):191-205.

3. Opstad KS, Wright AJ, Bell BA, Griffiths JR, Howe FA Correlations between in vivo (1)H MRS and ex vivo (1)H HRMAS metabolite measurements in adult human gliomas.. J Magn Reson Imaging. 2010; 31:289-297.

4. Martínez-Bisbal MC, Esteve V, Martínez-Granados B, Celda B. Magnetic resonance microscopy contribution to interpret high-resolution magic angle spinning metabolomic data of human tumor tissue. J Biomed Biotechnol. 2011;2011. pii: 763684. Epub 2010.

5. Barton SJ, Howe FA, Tomlins AM,Cudlip SA, Nicholson JK, Bell BA, Griffiths JR. Comparison of in vivo ^{1}H MRS of human brain tumours with ^{1}H HR-MAS spectroscopy of intact biopsy samples in vitro. Magnetic Resonance Materials in Physics, Biology and Medicine.1999; 8:121-128.

6. Cheng LL, Anthony DC, Comite AR, Black PM, Tzika AA, Gonzalez RG. Quantification of microheterogeneity in glioblastoma multiforme with ex vivo high-resolution magic-angle spinning (HRMAS) proton magnetic resonance spectroscopy. Neuro Oncol 2000;2:87–95.

7. Tugnoli V, Schenetti L, Mucci A, Parenti F, Cagnoli R, Righi V, Trinchero A, Nocetti L, Toraci C, Mavilla L, Trentini G, Zunarelli E, and Tosi MR. Ex vivo HR-MAS MRS of human meningiomas: a comparison with in vivo ^{1}H MR spectra. Int. J. Mol. Med. 2006; 18,: 859–869.

8. Tzika AA, Astrakas L, Cao H, Mintzopoulos D, Andronesi OC, Mindrinos M, Zhang J, Rahme LG, Blekas KD, Likas AC, Galatsanos NP, Carroll RS, Black PM. Combination of high-resolution magic angle spinning proton magnetic resonance spectroscopy and microscale genomics to type brain tumor biopsies. Int J Mol Med. 2007;20(2):199-208.

9. Righi V, Roda JM, Paz J, Mucci A, Tugnoli V, Rodriguez-Tarduchy G, Barrios L, Schenetti L, Cerdan S, Garcia-Martin ML. ^{1}H HR-MAS and genomic analysis of human tumor biopsies discriminate between high and low grade astrocytomas. NMR Biomed. 2009; 22:629-637.

10. Wright AJ, Fellows G, Byrnes TJ, Opstad KS, McIntyre DJ, Griffiths JR, Bell BA, Clark CA, Barrick TR, Howe FA, attern recognition of MRSI data shows regions of glioma growth that agree with DTI markers of brain tumor infiltration, Magn Reson Med. 2009;62(6):1646-51.

11. Lopez-Gines C, Gil-Benso R, Faus C, Monleon D, Mata M, Morales JM, Cigudosa JC, Gonzalez-Darder J, Celda B, Cerda-Nicolas M. Metastasizing anaplastic ependymoma in an adult. Chromosomal imbalances, metabolic and gene expression profiles. Histopathology. 2009 Mar;54(4):500-4.

12. Ferrer-Luna R, Mata M, Núñez L, Calvar J, Dasí F, Arias E, Piquer J, Cerdá-Nicolás M, Taratuto AL, Sevlever G, Celda B, Martinetto H. Loss of heterozygosity at 1p-19q induces a global change in oligodendroglial tumor gene expression. J Neurooncol. 2009 Dec; 95(3):343-54.

13. Lopez-Gines C, Gil-Benso R, Ferrer-Luna R, Benito R, Serna E, Gonzalez-Darder J, Quilis V, Monleon D, Celda B, Cerdá-Nicolas M. New pattern of EGFR amplification in glioblastoma and the relationship of gene copy number with gene expression profile. Mod Pathol. 2010 Jun;23(6):856-65.

14. Ferrer-Luna R, Núñez L, Piquer J, Arias E, Dasí F, Cervio A, Arakaki N, Sevlever G, Celda B, Martinetto H. Whole-genomic survey of oligodendroglial tumors: correlation between allelic imbalances and gene expression profiles. J Neurooncol. 2010.

15. Devos A, Simonetti AW, van der Graaf M, Lukas L, Suykens JAK, Vanhamme L, Buydens LMC, Heerschap A, Van Huffel S. The use of multivariate MR Imaging Intensities versus metabolic data from MR Spectroscopic Imaging for brain tumour classification. J Magn Reson. 2005; 173: 218-228.

16. De Vos M, Laudadio T, Simonetti AW, Heerschap A, Van Huffel S. Fast nosologic imaging of the brain. J Magn Reson. 2007; 184: 292-301.

17. Simonetti AW, Melssen WJ, van der Graaf M, Heerschap A, Buydens LMC, A chemometric approach for brain tumor classification using magnetic resonance imaging and spectroscopy. Analytical Chemistry.2003; 75: 5352–5361.

18. Luts J, Laudadio T, Idema AJ, Simonetti AW, Heerschap A, Vandermeulen D, Suykens JAK, Van Huffel S. Nosologic imaging of the brain: segmentation and classification using MRI and MRSI. NMR Biomed. 2009;22(4):374-90.

19. Simonetti AW, Melssen WJ, Szabo de Edelenyi F, van Asten JA, Heerschap A, Buydens LMC, Combination of feature-reduced MR spectroscopic and MR imaging data for improved brain tumor classification. NMR Biomed. 2005; 18: 34–43.

20. Laudadio T, Pels P, De Lathauwer L, Van Hecke P, Van Huffel S, Tissue segmentation and classication of MRSI data using canonical correlation analysis. Magn Reson Med. 2005; 54: 1519–1529.

21. Laudadio T, Martinez-Bisbal MC, Celda B, Van Huffel S, Fast nosological imaging using canonical correlation analysis of brain data obtained by two-dimensional turbo spectroscopic imaging. NMR Biomed. 2008; 21: 311–321.

22. Golub GH, Van Loan CF, Matrix computations. The Johns Hopkins University Press, Baltimore. 1996.

23. Correa N, Li YO, Adalı T, and Calhoun VD, Canonical correlation analysis for feature-based fusion of biomedical imaging modalities and its application to detection of associative networks in schizophrenia, IEEE J. Select. Topics Signal Process. 2008; 2(6): 998–1007.

24. Correa N, Adalı T, Li YO, and Calhoun VD, Canonical Correlation Analysis for Data Fusion and Group Inferences, IEEE Signal Processing Magazine, 2010; 27(4) : 39 – 50.

25. Li YO, Wang, Adalı T, and Calhoun VD, Joint blind source separation by multi-set canonical correlation analysis, IEEE Trans. Signal Processing. 2009; 57(10):3918–3929.

26. Laudadio T, Mastronardi N, Vanhamme L, Van Hecke P and Van Hufel P. Improved Lanczos algorithms for blackbox MRS data quantitation. J Magn Reson 2002; 157: 292-297.

27. Croitor Sava AR, Martinez-Bisbal MC, Van Huffel S, Cerda JM, Sima DM, Celda B. Ex Vivo High Resolution Magic Angle Spinning Metabolic Profiles Describe Intratumoral Histopathological Tissue Properties in Adult Human Gliomas. Accepted for publication in Magn Reson Med. 2010.

28. Poullet JB. Quantification and Classification of Magnetic Resonance Spectroscopic Data for Brain Tumor Diagnosis. PhD thesis, Faculty of Engineering, K.U.Leuven.2008.

29. Friman O. Adaptive Analysis of Functional MRI Data . PhD thesis. Linköping University, Sweden, 2003.

30. Szabo de Edelenyi F, Rubin C, Esteve F, Grand S, Decorps M, Lefournier V, Le Bas JF, Remy C, A new approach for analyzing proton magnetic resonance spectroscopic images of brain tumors: nosologic images. Nature Medicine. 2000; 6: 1287–1289.

31. Guyon I, Alamdari ARSA, Dror G, Buhmann JM (2006) Performance Prediction Challenge. In: IJCNN ’06 international joint conference on neural networks, pp 1649–1656.

32. Lewicki P and Hill T, Statistics: Methods and Applications. StatSoft., 2006.

33. Waters NJ, Garrod S, Farrant RD, Haselden JN, Connor SC, Connelly J, Lindon JC, Holmes E. and Nicholson JK. High-Resolution Magic Angle Spinning ^{1}H NMR Spectroscopy of Intact Liver and Kidney: Optimization of Sample Preparation Procedures and Biochemical Stability of Tissue during Spectral Acquisition. Analytical Bio.